Physics and Chemistry of Minerals (2018) 45:563–574
https://doi.org/10.1007/s00269-018-0942-5

ORIGINAL PAPER

Autocorrelation analysis of the infrared spectra of synthetic and biogenic carbonates along the calcite–dolomite join

David M. Jenkins[1] · Zachary F. Holmes[1] · Kiyotaka Ishida[2] · Phillip D. Manuel[1]

Received: 24 October 2017 / Accepted: 12 January 2018 / Published online: 19 January 2018

Abstract

Autocorrelation analysis of infrared spectra can provide insights on the strain energy associated with cation substitutions along a solid-solution compositional join which to date has been applied primarily to silicate minerals. In this study, the method is applied to carbonates synthesized at 10 mol% increments along the calcite–dolomite ($CaCO_3$–$CaMg(CO_3)_2$) join in the range of 1000–1150 °C and 0.6–2.5 GPa for the purpose of determining how the band broadening in both the far- and mid-infrared ranges, as represented by the autocorrelation parameter $\delta\Delta$Corr, compares with the existing enthalpy of mixing data for this join. It was found that the carbonate internal vibration ν_2 (out-of-plane bending) in the mid-infrared range, and the sum of the three internal vibration modes $\nu_4+\nu_2+\nu_3$ most closely matched the enthalpy of mixing data for the synthetic carbonates. Autocorrelation analysis of a series of biogenic carbonates in the mid-infrared range showed only a systematic variation for the ν_2 band. Using the biogenic carbonate with the lowest Mg content for reference, the trend in $\delta\Delta$Corr for biogenic carbonates shows a steady increase with increasing Mg content suggesting a steady increase in solubility with Mg content. The results from this study indicate that autocorrelation analysis of carbonates in the mid-infrared range provides an independent and reliable assessment of the crystallographic strain energy of carbonates. In particular, inorganic carbonates in the range of 0–17 mol% $MgCO_3$ experience a minimum in strain energy and a corresponding minimum in the enthalpy of mixing, whereas biogenic carbonates show a steady increase in strain energy with increasing $MgCO_3$ content. In the event of increasing ocean acidification, biogenic carbonates in the range of 0–17 mol% $MgCO_3$ will dissolve more readily than the compositionally equivalent inorganic carbonates.

Keywords Magnesian-calcite · Synthetic carbonates · Autocorrelation analysis · Infrared spectroscopy · Biogenic carbonates · Enthalpy of mixing

Introduction

Autocorrelation analysis of the mid- and far-infrared (MIR and FIR) spectra of minerals has been used by a number of researchers to quantify such things as phase transitions, cation mixing in solid solutions, and order–disorder processes (Salje et al. 2000; Tarantino et al. 2002; Boffa Ballaran and Carpenter 2003; Etzel and Benisek 2008; Koch-Müller et al. 2012; Robben and Gesing 2013; Jenkins et al. 2014). In brief, autocorrelation analysis involves taking portions of a spectrum and correlating it to itself to produce the autocorrelated spectrum, Corr(α, ω'), using the autocorrelation function defined as (Salje et al. 2000):

$$\mathrm{Corr}(\alpha,\omega') = \int_{-\infty}^{\infty} \alpha(\omega+\omega')\alpha(\omega)\mathrm{d}\omega \quad (1)$$

where $\alpha(\omega)$ is the spectrum of interest and $\alpha(\omega+\omega')$ is that same spectrum offset in wavenumber or frequency by an amount ω'. The advantage of this method is that it can produce a symmetric spectrum from a potentially complex and asymmetric spectrum and allows one to compare, in a systematic manner, relative differences in the breadths of the vibrational spectra (via the parameter $\delta\Delta$Corr) caused by differences in lattice strain arising from order/disorder, compositional solid solution, phase transitions, etc. To date, there does not appear to be an absolute relationship between band

✉ David M. Jenkins
dmjenks@binghamton.edu

[1] Department of Geological Sciences and Environmental Studies, Binghamton University, Binghamton, NY 13902, USA

[2] Fukuoka, Japan

widening and the enthalpy of mixing for mineral solid solutions (Boffa Ballaran and Carpenter 2003) owing to the lack of a universal relationship between strain-induced structural changes and vibrational spectra broadening. Although some success was achieved by Etzel and Benisek (2008) in demonstrating a systematic relationship between the ratio of the enthalpy of mixing to $\delta\Delta$Corr and the integrated excess volume for several mineral solid solutions, this has not yet been shown to be applicable to all solid solutions (e.g., Jenkins et al. 2014). Therefore, autocorrelation analysis is less useful for extracting absolute enthalpies of mixing but more useful in determining relative differences in enthalpies of mixing along a solid-solution join, particularly given the high precision of this technique compared to solution calorimetric methods (Boffa Ballaran and Carpenter 2003). It has been found that the autocorrelation spectra of synthetic materials are particularly useful for comparative purposes and are not strongly influenced by user-controllable parameters, such as sample grinding time, infrared (IR) pellet preparation and dilution, and instrument resolution (Blanch et al. 2007).

The purpose of this study is twofold. First, the MIR and FIR spectra of a series of synthetic (hexagonal) carbonates along the calcite–dolomite ($CaCO_3$–$CaMg(CO_3)_2$) join are analyzed by autocorrelation analysis to determine if the observed $\delta\Delta$Corr values replicate the enthalpies of mixing reported for this join (Navrotsky and Capobianco 1987; Chai et al. 1995). Particular attention will be given to see if both the MIR and FIR ranges replicate the negative deviations reported by Navrotsky and Capobianco (1987) to determine what, if any, vibrational length scale duplicates the enthalpies of mixing. Second, the MIR spectra of a series of modern biogenic carbonates are also analyzed by autocorrelation analysis to use the greater precision of this method to help determine if a negative deviation in the enthalpy of mixing exists for magnesian calcites, suggesting the presence of a limited range of low-Mg biogenic carbonates that would be less soluble than others.

Methods

Carbonate synthesis

All carbonates on the $CaCO_3$–$CaMg(CO_3)_2$ join were synthesized from mixtures of synthetic $CaCO_3$ and $MgCO_3$. The former was low-alkali $CaCO_3$ (Baker Analyzed reagent) used as provided, while the latter was made as follows: Reagent-grade MgO (Aldrich) was mixed with (nominally) anhydrous oxalic acid ($H_2C_2O_4$) in the molar ratio of approximately 1 MgO:0.7 $H_2C_2O_4$. This mixture was placed in an unsealed gold or silver-palladium ($Ag_{50}Pd_{50}$) capsule and treated at 0.6 GPa and 650 °C for 22 h in the presence of an approximately equimolar ratio of CO_2:Ar gas in an internally heated gas vessel (described below). The resultant $MgCO_3$ was slightly grey in color but otherwise was single-phase magnesite based on its X-ray diffraction pattern. Intermediate carbonates were then made from mixtures of $CaCO_3$ and $MgCO_3$ which were sealed in platinum capsules as either a dry mixture or with minor amounts (5–20 wt%) of H_2O, oxalic acid dihydrate ($H_2C_2O_4{\cdot}2H_2O$), or anhydrous oxalic acid. The H_2O was added to provide a flux, while the oxalic acid dihydrate or anhydrous oxalic acid was used to provide some water and sufficient CO_2 partial pressure to prevent the sample from decarbonating. It might be noted that attempts to make intermediate carbonates using commercially available hydrous magnesite ($MgCO_3{\cdot}nH_2O$) instead of synthetic anhydrous $MgCO_3$ generally produced poor yields of the desired carbonate coexisting with abundant brucite and/or periclase.

Experimental apparatus

Carbonates in the compositional range of pure $CaCO_3$ to $(CaCO_3)_{70}{\cdot}(MgCO_3)_{30}$ as well as pure magnesite ($MgCO_3$) were made in internally heated gas vessels using argon or, in some cases, a mixture of argon and carbon dioxide as the pressure medium. Capsules containing the sample were situated between two Inconel®-sheathed chromel–alumel thermocouples to observe the temperature gradient along the capsule. Uncertainties in reported temperatures reflect both the uncertainty in calibration (± 2 °C, calibrated against the freezing point of NaCl) and any thermal gradient across the sample. Pressures were measured with bourdon-tube gauges, calibrated against Harwood factory-calibrated manganin-cell resistance pressure gauges, and are considered accurate to ± 0.005 GPa. Carbonates whose compositions were between $(CaCO_3)_{75}{\cdot}(MgCO_3)_{25}$ and $(CaCO_3)_{50}{\cdot}(MgCO_3)_{50}$ (dolomite) were made in a piston-cylinder press using pressure media made of NaCl for experiments up to 1000 °C or of $SrCO_3$ for experiments above 1000 °C. Pressures are considered accurate to ± 0.05 GPa and temperatures to ± 10 to ± 15 °C for experiments done in the ranges of 1000–1150 °C, respectively.

Analytical methods

Powder X-ray diffraction (XRD) was used both to determine the products of synthesis and to determine the compositions of the carbonate solid solutions. Powder diffraction patterns were obtained on a Panalytical PW3040-MPD diffractometer operated at 40 kV and 20 mA with Cu radiation and fitted with a graphite-diffracted-beam monochrometer to filter all but Kα radiation. Samples were mounted on zero-background single-crystal quartz plates. To improve measurement consistency, about 5–10 wt% NaCl ($a_0 = 5.6401$ Å) was mixed in with the carbonate sample and the observed pattern

corrected to the internal standard NaCl peak positions. Compositions of the synthetic carbonate solid solutions were determined using the calibration given by Titschack et al. (2011). These authors reported unit-cell dimensions for a series of echinoid remains spanning the range of 2–15 mol% $MgCO_3$. They then combined these data with all extant calibrations (via biogenic and synthetic carbonates) and derived linear correlations with unit-cell data that spanned the entire range from 0 to 50 mol% $MgCO_3$, i.e., from calcite to dolomite. Using unit-cell volumes, the uncertainties (99% confidence) in their calibration vary from about ± 1% in the range of 0–30 mol% $MgCO_3$ and gradually increasing up to about ± 2% for dolomite. Unit-cell dimensions for the samples formed in this study were determined using Rietveld structure refinements using the program GSAS (Larson and Von Dreele 2004) and initiated with the Mg-calcite structure of Althoff (1977). The unit-cell volumes were used to extract the mol% of $MgCO_3$; however, to minimize inter-laboratory differences, the volume for end-member calcite of Titschack et al. (2011) was adjusted to match the volume of pure calcite observed in this lab (366.79 $Å^3$), and this constant correction to volume was applied across the whole range of solid solutions. The resultant equation relating the unit-cell volume (V) to composition used in this study is:

$$\text{mol\% } MgCO_3 = 393.278 - 1.07222 \cdot \left(V,\ A^3\right) \quad (2)$$

Inorganic and biogenic carbonates were analyzed by electron probe microanalysis (EPMA) as well as by X-ray diffraction. For electron probe microanalysis, portions of the carbonates were mounted in epoxy, polished to 0.5 µm diamond grit, and carbon coated. Analysis was done with a JEOL 8900 electron microprobe operated at 15 kV and 10 nA using wavelength-dispersive spectroscopy using the ZAF matrix correction scheme (e.g., Reed 1996, pp. 134–140). Standards were $CaCO_3$ for Ca and dolomite for Mg. For biogenic carbonates, the calibration of volume versus mol% $MgCO_3$ determined by Mackenzie et al. (1983) was used in this study without applying any inter-laboratory corrections.

MIR spectra (4000–400 cm^{-1}) were measured in transmission mode using powdered samples embedded in KBr discs. Discs were prepared by mixing 1 mg of sample with 200 mg of KBr and pressed into 13 mm diameter discs under vacuum. Spectra were measured on a Bruker Equinox 55 FTIR under flowing nitrogen using 64 scans at 2 cm^{-1} resolution. FIR spectra (650–50 cm^{-1}) were measured (at Kyushu University) in transmission mode using sample discs consisting of 0.9–1.1 mg of sample embedded in about 80 mg polyethylene. Spectra were measured on a JASCO FTIR-620 fitted with a globar source using a PE-TGS detector with a PE-window and using a 5 µm mylar beam splitter. After the sample chamber was evacuated, 512 scans per sample were done at a nominal resolution of 4 cm^{-1}. Autocorrelation analysis was done using the software IGOR Pro version 6.2.10 using selected ranges of both the MIR and FIR ranges.

Results

Carbonate synthesis

Considerable care was used in finding the synthesis conditions that yielded essentially pure (hexagonal) carbonate, as determined from powder X-ray diffraction patterns. Table 1 is a summary of the synthesis experiments and conditions used, including those that did not yield pure carbonate, to provide the interested reader with information on what methods were found to be successful in this study. Treatment in the presence of H_2O often yielded a second coexisting phase (periclase, brucite, nesquehonite). In general, single-phase carbonates could be made by treating synthetic $CaCO_3$ and $MgCO_3$ in the presence of minor (10 wt%) oxalic acid dihydrate ($H_2C_2O_4{\cdot}2H_2O$) for mixtures with lower (< 30 mol%) $MgCO_3$ content and in the presence of (nominally) anhydrous oxalic acid ($H_2C_2O_4$, though loss on ignition suggests the presence of ~ 0.2 mols H_2O) for mixtures with higher (≥ 30 mol%) $MgCO_3$ content. Retreating the products of a previous synthesis attempt, which was found to be very useful for some silicates (e.g., glaucophane, Jenkins and Corona 2006), was generally less useful than establishing the correct chemical conditions. The most Mg-rich carbonates were made in the range of 2.1–2.5 GPa and 1000–1150 °C, where, based on the study of Irving and Wyllie (1975), single-phase (hexagonal) carbonate is stable relative to the dolomite–Mg-carbonate solvus at lower temperatures and the carbonate solidus at higher temperatures. The specific samples used for autocorrelation analysis are given in italics in Table 1.

Characterization of synthetic carbonates

Unit-cell dimensions and volumes of selected synthetic carbonates were determined using powder X-ray diffraction patterns as described above and are listed in Table 2. Systematic decreases in the cell dimensions and volumes were observed with increasing Mg content. One of the samples made from the Mg30Ca70 bulk composition (Mg30Ca70-4-1) was found to consist of two carbonates, as evidenced by splitting of the X-ray peaks that is unrelated to Cu $K_{\alpha1}$ and $K_{\alpha2}$ peak splitting. The refined compositions of the individual carbonates straddle the bulk composition of the mixture. Using the results from Rietveld refinement, the proportions of the higher- and lower-Mg carbonates are 56 ± 1.2 and 44 ± 1.3 wt%, respectively. Using the compositions of the carbonates listed in Table 2 and these wt% proportions, the bulk composition of the two carbonates combined is

Table 1 Synthesis conditions for carbonates made along the calcite–dolomite join

Sample code	T (°C)	P (GPa)	Time (h)	Fluid added (wt%)	Products
Mg0Ca100-1-1	1000 (10)	0.600 (20)	22	10% dihyd	Calcite
Mg5Ca95-1-1	1010 (11)	0.602 (5)	12	10% dihyd	Carbonate
Mg10Ca90-2-2	1010 (11)	0.603 (5)	12	5% H_2O	Carbonate + brucite
Mg10Ca90-2-3	1005 (5)	0.625 (5)	12	5% H_2O	Carbonate + brucite
*Mg10Ca90-2-4**	1000 (10)	0.620 (5)	22	5% H_2O	Carbonate
Mg15Ca85-1-1	1010 (10)	0.600 (20)	22	10% dihyd	Carbonate
Mg20Ca80-2-1	1004 (5)	0.619 (5)	22	15% H_2O	Carbonate + periclase
Mg20Ca80-2-2	1000 (2)	0.600(5)	22	20% H_2O	Carbonate + nesquehonite
Mg20Ca80-2-3	1000 (2)	0.608 (5)	22	10% H_2O	Carbonate + brucite
Mg20Ca80-2-4	1011 (12)	0.627 (5)	22	10% dihyd	Carbonate
Mg25Ca75-1-1	1050 (10)	2.13 (4)	22	10% dihyd	Carbonate
Mg30Ca70-2-1	1000 (10)	0.610 (5)	22	15% H_2O	Carbonate + periclase
Mg30Ca70-2-2	993 (7)	0.625 (5)	22	20% H_2O	Carbonate + periclase
Mg30Ca70-4-1	1150 (15)	2.50 (4)	6	10% anhyd	Carbonates (two)
Mg30Ca70-4-2	1100 (15)	1.97(5)	12	10% anhyd	Carbonate
Mg35Ca65-1-1	995 (8)	0.605(5)	12	None	Carbonate + brucite
Mg35Ca65-2-1	1000 (10)	2.11 (4)	22	10% dihyd	Carbonate + brucite
Mg35Ca65-2-2	1150 (15)	2.50 (4)	6	10% anhyd	Carbonate
Mg40Ca60-1-1	1000 (5)	0.612 (5)	22	10% dihyd	Carbonate + periclase
Mg40Ca60-1-2	1000 (10)	2.14 (4)	6	10% dihyd	Carbonate
Mg45Ca55-1-1	1150 (15)	2.11 (40)	24	10% anhyd	Carbonate + brucite
Mg45Ca55-1-2	1150 (15)	2.50 (5)	6	10% anhyd	Carbonate + brucite
*Mg45Ca55-1-3**	1150 (15)	2.50 (5)	6	10% anhyd	Carbonate
Mg50Ca50-1-1	1050 (10)	2.20 (4)	22	10% dihyd	Carbonate + brucite
Mg50Ca50-1-2	1150 (15)	2.45(5)	6	10% anhyd	Carbonate

Mixture bulk compositions (mol%) are indicated by the sample-code prefix

Uncertainties in the last digit are given in parentheses. Sample codes given in italics indicate those samples used for autocorrelation analysis. All carbonates formed are hexagonal

Anhyd, oxalic acid anhydrate (nominal); dihyd, oxalic acid dihydrate

*Retreatment of synthesis products of previous sample

31.4 ± 1 mol% $MgCO_3$, which is nearly the same as that of the starting mixture. A duplicate synthesis on this bulk composition (Mg30Ca70-4-2, Table 1) was found to yield a single-phase carbonate. Care was exercised in looking at the other samples for evidence of coexisting carbonates, but only sample Mg30Ca70-4-1 appeared to have coexisting carbonates. Figure 1 shows the compositions of the synthetic carbonates made in this study as determined using Eq. (2). The sample that yielded two carbonates is shown by the squares. Although there is some scatter about the 1:1 correlation line, the agreement is very good.

Rietveld refinements of all of the synthetic carbonates, except for those of dolomite composition (Mg50Ca50-1-2 and natural dolomite), were done using the calcite structure ($R\bar{3}c$) appropriate for disordered rhombohedral carbonates. There was no indication of the b-type ordering reflections (Goldsmith and Heard 1961; Reeder and Nakajima 1982) arising from the ordered structure of dolomite ($R\bar{3}$) in the synthetic carbonates, even for bulk compositions through 45 mol% $MgCO_3$. For the dolomite bulk compositions, the Ca-Mg order/disorder parameter s was estimated as $s = \sqrt{I_{10\bar{5}}/I_{006}}$ (Zucchini et al. 2012), where $I_{10\bar{5}}$ and I_{006} are the integrated areas of the $10\bar{5}$ and 006 reflections, respectively. This method was chosen rather than using the site occupancy of Ca at the crystallographic A site ($s = (2 \cdot X^{A}_{Ca} - 1)$) because of the low accuracy of site occupancies obtained from Rietveld refinements of powder patterns that are not measured in a high-resolution mode (Antao et al. 2008). The ordering parameter, which ranges from 1.0 to 0.0 for fully ordered to disordered structures, respectively, is indicated in Table 2. For the natural inorganic dolomite, the observed value of 1.09 is beyond the expected range but is consistent with the high values observed for other dolomite samples (Antao et al. 2004; Zucchini et al. 2012) and, in this case, may be influenced by preferred orientation. For the synthetic dolomite, the observed value of 0.76 indicates partial disorder and is consistent with the values observed in dolomite treated

Table 2 Unit-cell dimensions, volumes, position of the (104) XRD reflection, full-width at half maximum (FWHM) of the (104), and calculated mole% of $MgCO_3$ of selected synthetic and inorganic carbonates

Sample code	a_0 (Å)	c_0 (Å)	V (Å^3)	°2θ (104)	FWHM (°2θ)	$MgCO_3$ (mol%)
Mg0Ca100-1-1	4.9859 (3)	17.037 (2)	366.79 (5)	29.38	0.122	0.0 ± 1.0
Mg5Ca95-1-1	4.9644 (4)	16.933 (2)	361.41 (5)	29.60	0.122	5.8 ± 1.0
Mg10Ca90-2-4	4.9543 (4)	16.893 (2)	359.10 (3)	29.63	0.122	8.2 ± 1.0
Mg15Ca85-1-1	4.9314 (10)	16.784 (4)	353.47 (6)	29.87	0.200	14.3 ± 1.0
Mg20Ca80-2-4	4.9095 (11)	16.657 (4)	347.69 (6)	29.99	0.158	20.5 ± 1.0
Mg25Ca75-1-1	4.8903 (8)	16.583 (3)	343.46 (5)	30.12	0.140	25.0 ± 1.0
Mg30Ca70-4-1[a]	4.856 (1)	16.403 (4)	334.95 (7)	30.38	0.149	34.1 ± 1.2
	4.881 (2)	16.516 (6)	340.80 (9)	30.19	0.168	27.9 ± 1.0
Mg30Ca70-4-2	4.8632 (5)	16.447 (2)	336.88 (3)	30.35	0.131	32.1 ± 1.1
Mg35Ca65-2-2	4.8609 (12)	16.414 (4)	335.88 (7)	30.46	0.200	33.1 ± 1.2
Mg40Ca60-1-2	4.8354 (9)	16.256 (3)	329.18 (5)	30.61	0.149	40.3 ± 1.5
Mg45Ca55-1-3	4.8202 (6)	16.164 (2)	325.24 (3)	30.74	0.131	44.5 ± 1.7
Mg50Ca50-1-2[b]	4.8018 (4)	16.023 (1)	319.96 (3)	31.03	0.149	50.2 ± 2.0
Calcite[c]	4.9876 (1)	17.0547 (7)	367.41 (2)	29.41	0.149	0.33 ± 0.05[c]
Dolomite[b,c]	4.8064 (2)	16.009 (1)	320.29 (2)	30.95	0.149	49.8 ± 0.3[c]

Uncertainties (1σ) in the last digit of the cell dimensions and volumes are given in parentheses. Uncertainties in the $MgCO_3$ contents are discussed in the "Methods" section

[a]Two carbonates appeared in this sample, evidenced by splitting of the XRD peaks. Refined proportions of the higher- and lower-Mg carbonates are 56 ± 1.2 and 44 ± 1.3 wt%, respectively

[b]Observed ordering parameter for Mg50Ca50-1-2 is $s = 0.76$, and for inorganic (natural) dolomite $s = 1.09$

[c]Calcite is optical grade (unknown locality). Dolomite is from Butte, MT, sample 49E5871 of Ward's Natural Science, Inc. Compositions for calcite and dolomite are from EPMA; the amount of $FeCO_3$ in calcite is below the detection limit and is 1.1 ± 0.4 mol% in dolomite

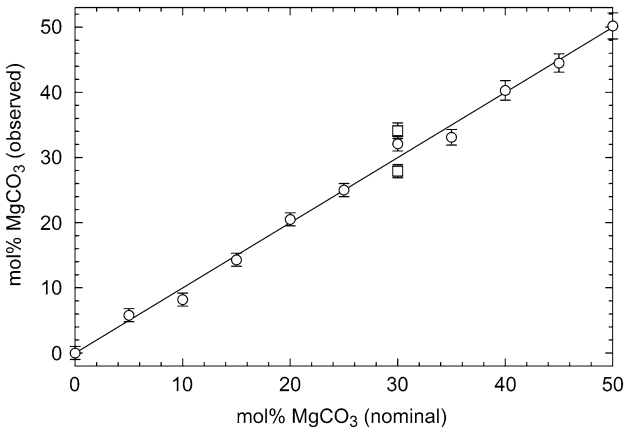

Fig. 1 Observed versus nominal carbonate bulk composition for selected synthetic carbonates listed in Table 2. Compositions were determined from Eq. (2) in the text, where it should be noted that only the Mg-free sample (synthetic calcite) was used to account for inter-laboratory differences between the study of Titschack et al. (2011) and this one. The diagonal line represents 1:1 correlation

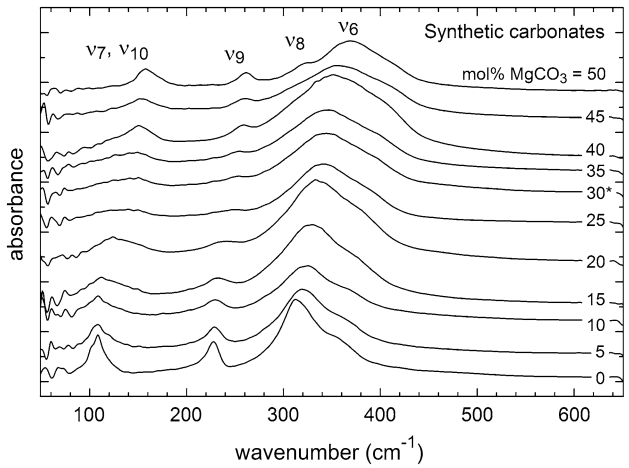

Fig. 2 The far-infrared (75–400 cm^{-1}) and part of the mid-infrared (400–600 cm^{-1}) absorption spectra for the synthetic carbonates made in this study. Labels indicate the mol% of $MgCO_3$ in the sample, while the band assignments are those of White (1974) and Andersson et al. (2014)

and quenched from high temperatures (Reeder and Wenk 1983).

Figure 2 shows the spectra obtained at 75–600 cm^{-1} which includes the FIR (75–400 cm^{-1}) and a portion of the MIR (400–600 cm^{-1}) ranges, the latter being featureless in this range. The FIR bands are assigned to lattice vibration modes with the lowest frequency bands (ν_7 and ν_{10}) attributed to rotational motions of the carbonate group and the higher frequency bands (ν_9, ν_8, and ν_6) to translatory motions of the Ca(+Mg) and carbonate group (White 1974; Andersson et al. 2014). Compared to the MIR spectra discussed below, the FIR spectra show systematic shifts in the band

widths and positions, with a gradual shift in all bands to higher frequencies (larger wavenumbers) with increasing Mg content and a noticeable widening of the lower frequency bands near the middle of the compositional join. It should be noted that the spectrum for the Mg30 bulk composition (marked by an asterisk) is that of the two-carbonate mixture (sample Mg30Ca70-4-1, Table 1); the spectrum for the single-carbonate sample (Mg30Ca70-4-2, Table 1) was measured at a much later date than the original series of FIR spectra and, for reasons that are not clear, has an FIR spectrum that is not consistent with carbonates (Brusentsova et al. 2010). At this time, it can only be assumed that the small amount of sample Mg30Ca70-4-1 available for FIR analysis was contaminated with some non-carbonate material in transit to Kyushu University and subsequently was not used. The consistent variations in the series of FIR spectra in Fig. 2 combined with the compositional similarity of the two carbonates in this sample (Table 2) suggests that including the spectrum of the two-carbonate mixture should be adequate for the purposes of autocorrelation analysis. As will be seen later, this two-carbonate sample could be deleted entirely from the FIR series and it will not fundamentally change the conclusions.

MIR spectra of the synthetic carbonates are shown in Fig. 3. The spectra in this range (500–2500 cm^{-1}) are relatively simple, consisting of the two lower-intensity bands ν_4 and ν_2, assigned to in-plane and out-of-plane bending of C–O bonds, respectively, and the dominant ν_3 band, which is assigned to the anti-symmetric stretching of C–O bonds. All three of these are infrared-active internal vibration modes of the CO_3^{-2} group (White 1974; Andersson et al. 2014). Across this join, there is relatively little change in band positions; however, there is a noticeable change in band widths and relative intensities, with the bands becoming widest in the 30–40 mol% $MgCO_3$ range.

Autocorrelation analysis of synthetic carbonates

Portions of the FIR and MIR spectra to which linear backgrounds could be readily fitted were analyzed by the autocorrelation method and are shown in Figs. 4 and 5. Starting with the FIR spectra, the spectra were divided into two ranges: (a) one that is 92 cm^{-1} wide and encompasses the lattice modes ν_7 and ν_{10} (rotational bands), with maxima varying from 107 to 157 cm^{-1}; and (b) a second range that is 338 cm^{-1} wide and encompasses the lattice modes ν_9, ν_8, and ν_6 (translatory bands), which shift 20–35 cm^{-1} to higher frequencies with increasing Mg content. Using the method described in detail in Salje et al. (2000), autocorrelation analysis was performed on these two ranges and the resulting values of $\delta\Delta$Corr are shown in Fig. 4a, b, respectively. Both of these ranges display a fairly symmetric maximum in $\delta\Delta$Corr, indicating a maximum in crystal strain near the middle of the compositional join. There is a possible local minimum at 50 mol% $CaMg(CO_3)_2$ in Fig. 4b. This may arise from the presence of the ordered superstructure "γ dolomite" reported by Wenk and Zhang (1985), which has the same bulk composition ($Ca_{0.75}Mg_{0.25}CO_3$), and may produce a local minimum in the Gibbs free energy curve, as proposed by Wenk and Zhang (1985), and observed here as a local minimum in the $\delta\Delta$Corr curve which proxies for the ΔH^{mix} behavior. Additional samples at smaller compositional intervals through this region of the join would be needed to confirm the presence of this minimum.

For the MIR spectral range, all three internal vibration modes ν_4, ν_2, and ν_3 were first analyzed separately, owing

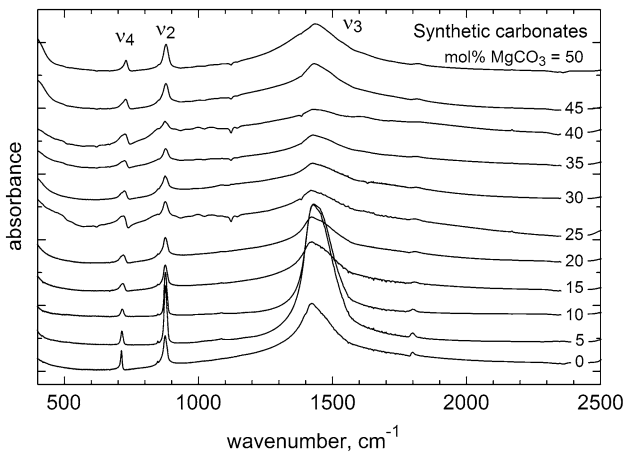

Fig. 3 Mid-infrared absorption spectra for the synthetic carbonates made in this study including the single-phase carbonate for the 30 mol% composition. Labels same as those in Fig. 2, with the band assignments of White (1974) and Andersson et al. (2014)

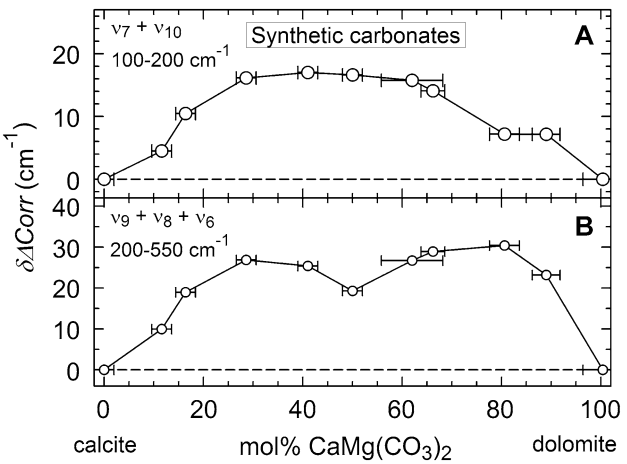

Fig. 4 **a** Autocorrelation parameter $\delta\Delta$Corr for the $\nu_7+\nu_{10}$ lattice rotational modes in the FIR range of 100–200 cm^{-1}. **b** $\delta\Delta$Corr for the $\nu_9+\nu_8+\nu_6$ lattice translatory modes in the FIR range of 200–550 cm^{-1}

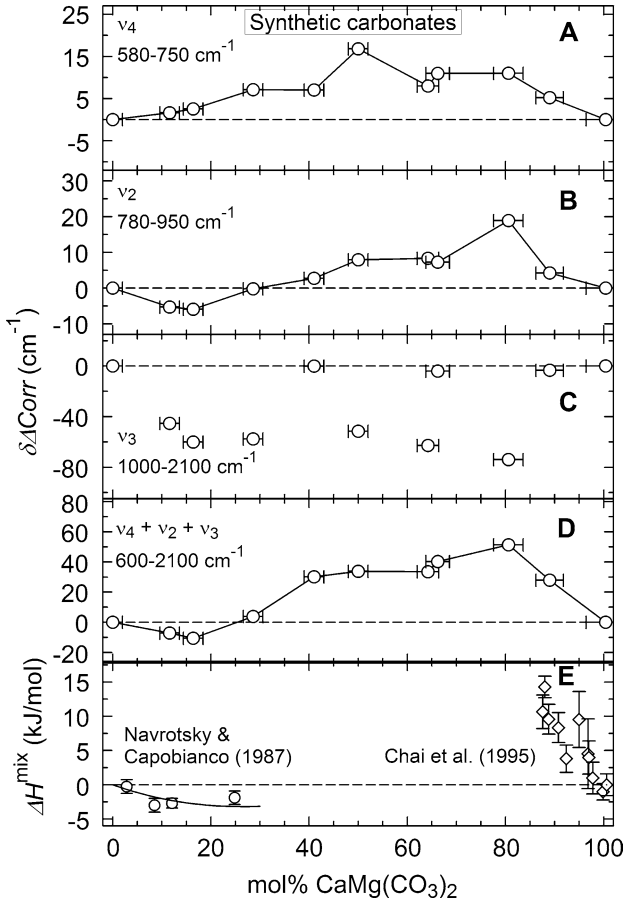

Fig. 5 **a** Autocorrelation parameter $\delta\Delta$Corr for the internal vibration mode ν_4 in the range of 580–750 cm^{-1}. **b** $\delta\Delta$Corr for the internal vibration mode ν_2 in the range of 780–950 cm^{-1}. **c** $\delta\Delta$Corr for the internal vibration mode ν_3 in the range of 1000–2100 cm^{-1}. **d** $\delta\Delta$Corr for the sum of the internal vibration modes $\nu_4+\nu_2+\nu_3$ in the range of 600–2100 cm^{-1}. **e** Solution calorimetry values for synthetic carbonates reported by Navrotsky and Capobianco (1987, circles) and Chai et al. (1995, diamonds)

to the lack of band overlap and very limited frequency shift, and then analyzed together in the range of 610–2100 cm^{-1}. The results are shown in Fig. 5a–d and the frequency ranges of the autocorrelation analysis indicated on the figures. Unlike the symmetric curves observed for the two FIR lattice vibration ranges (Fig. 4a, b), these curves are distinctly asymmetric. The ν_4 band, like the FIR bands, shows positive deviations from the end-members across the entire join but with the Mg-rich compositions having more positive values than the Mg-poor compositions. The ν_2 band shows a decrease in $\delta\Delta$Corr going from pure calcite out to about 20 mol% $CaMg(CO_3)_2$ and then crossing over to positive values at about 30 mol% $CaMg(CO_3)_2$ and reaching a maximum at 80 mol%. The ν_3 band, the strongest in the MIR range, also starts out with a decrease in $\delta\Delta$Corr but, even though it remains negative, displays irregular variations in $\delta\Delta$Corr with increasing Mg content. The origin of this behavior is unknown but is tentatively attributed to the same sort of fine structure that is observed in the FTIR thin-layer microscopy analysis of the ν_4 and ν_2 bands in synthetic magnesian calcites, and appears for the ν_3 band in KBr pellet mounts (Long et al. 2012, Fig. S2). Such fine structure could lead to low values of $\delta\Delta$Corr (i.e., narrow maxima in the autocorrelated spectra) for certain compositions.

Recognizing that $\delta\Delta$Corr can not yet be directly translated into absolute values for the enthalpy of mixing (Boffa Ballaran and Carpenter 2003; Etzel and Benisek 2008), some success has been realized in using the $\delta\Delta$Corr curve to indicate the sense of asymmetry or shed light on the enthalpy and perhaps Gibbs-free energy of mixing for the tremolite–glaucophane (Jenkins et al. 2014) and hornblende–glaucophane (Lei et al. 2015) joins, respectively. For this study, an important piece of information is available, namely the enthalpies of solution have been measured for synthetic Mg-calcites (Navrotsky and Capobianco 1987; Bishoff 1998) and Ca–dolomites (Chai et al. 1995) from which the ΔH^{mix} can be derived. The results of Navrotsky and Capobianco (1987) based on HCl-acid solution calorimetry at 85 °C are shown in Fig. 5e, which are similar to the results of Bishoff (1998) obtained from acetic acid solution calorimetry at 25 °C. In view of this information, it is now possible to identify which portion(s) of the infrared spectrum most closely agree with the measured enthalpies of mixing and thereby identify the length scale over which compositionally induced strain operates (Carpenter 2002). Based on the autocorrelation results shown in Figs. 4 and 5, it is only the internal vibration ν_2 (Fig. 5b) and the composite of all internal vibrations $\nu_4+\nu_2+\nu_3$ (Fig. 5d) which show the negative deviation from ideality for the low-Mg compositions and positive deviation for high-Mg compositions. The main conclusion is that only autocorrelation of the MIR range is providing an accurate representation of the experimentally measured enthalpies of mixing shown in Fig. 5e, suggesting the scale of compositionally induced strain is sensed by the internal rather than lattice vibration modes.

Characterization of biogenic carbonates

A series of modern marine carbonates was selected for this study and are listed in Table 3. Portions of the tests or spines were analyzed both by powder X-ray diffraction as described in the "Methods" section (using NaCl as an internal standard) as well as by electron microprobe analysis. The unit-cell volume calibration curve reported by Mackenzie et al. (1983) for biogenic carbonates was used here. The electron microprobe and X-ray diffraction-based analyses are in very close agreement, with only the most Mg-rich sample showing any significant deviation. This lack of agreement at the highest Mg content may arise from using the non-linear curve reported by Mackenzie et al. (1983) at the limit of its

Table 3 Biogenic Mg-calcites used in this study, in order of increasing Mg content

Sample code	Common name	Species
PML-1	Periwinkle	*Littorina littorea*
PMC-1	Atlantic oyster	*Crassostrea virginica*
PMBS-1	Bay scallop	*Argopecten irradians*
PMM-1	Sea urchin spine	*Echinoid sp.*
PMSD-1	Sand dollar	*Mellita sp.*
PMH-1	Foraminifer	*Homotrema rubrum*
PMU-1	Sea biscuit	*Clypeaster sp.*
PMR-1	Red algae	*Lithothamnion sp.*

calibration. For this study, the electron microprobe (EPMA) results are used as listed in Table 3.

Autocorrelation analysis of biogenic carbonates

Based on the results observed here for synthetic carbonates, namely that variation in the enthalpy of mixing is accurately reflected in the MIR range, the infrared spectra in the MIR range for the biogenic carbonates listed in Table 4 were measured and are shown in Fig. 6. Additionally shown in Fig. 6 are the spectra of natural inorganic (abiotic) calcite and dolomite which might be considered reference points for the biogenic carbonates. The spectra of all the carbonates are arranged in order of increasing Mg content from top to bottom. Autocorrelation analysis of the ν_4, ν_2, and ν_3 bands as a single group is shown in Fig. 7a, referenced to the dashed line between inorganic calcite and dolomite (off scale to the right). Unlike synthetic carbonates (Fig. 5d), there is no apparent trend in $\delta\Delta$Corr with composition for biogenic carbonates. The origin of this lack of correlation is unknown but is tentatively attributed to greater development of fine structure (Long et al. 2012) in the strong ν_3 band for biogenic compared to synthetic carbonates. Autocorrelation values extracted from the ν_2 band in Fig. 7b, however, show a more systematic trend. Adopting inorganic

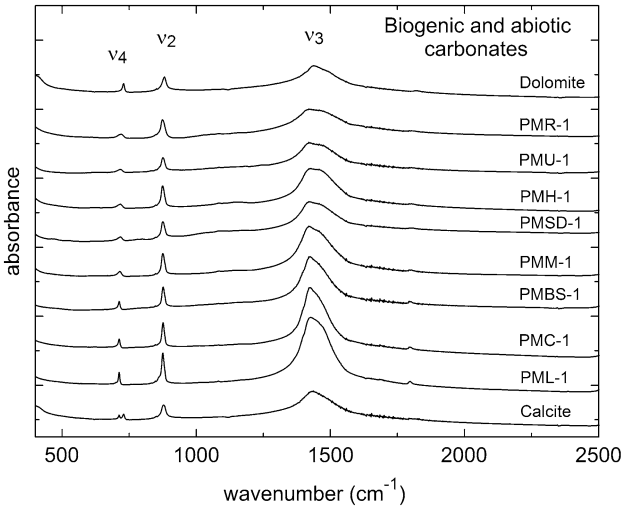

Fig. 6 Mid-infrared absorption spectra for the biogenic carbonates listed in Table 3, listed in order of decreasing Mg contents from top to bottom, along with the spectra of natural inorganic calcite (locality unknown), and dolomite (Butte, MT, USA)

calcite and dolomite as the baseline, the $\delta\Delta$Corr values drop quickly going from the calcite to the first biogenic sample followed by a gradual rise to the baseline (with dolomite) for the most Mg-rich composition. This region of negative deviation occurring between 0 and 30 mol% $CaMg(CO_3)_2$ is similar to that shown by the ν_2 band for synthetic carbonates in Fig. 5b. Inorganically formed calcite may not be a good analogue for Mg-free biogenic carbonates as it ignores contributions from any vital effects, such as the incorporation of amorphous carbonates or occluded macromolecules (Weiner and Dove 2003), in which case choosing the sample with the lowest Mg content (PML-1) for establishing the baseline along with dolomite might be more reasonable. Figure 7c shows the values of $\delta\Delta$Corr referenced to this baseline; there is little, if any, range over which there is a negative deviation in $\delta\Delta$Corr. This last version agrees with the ΔH^{mix} derived from the enthalpies of solution for

Table 4 Compositions of biogenic carbonates based on XRD and EPMA analysis

Sample code	XRD				EPMA (mol)		
	a (Å)	c (Å)	V (Å^3)	$MgCO_3$ (mol%)	$CaCO_3$	$MgCO_3$	$SrCO_3$
PML-1	4.9866 (3)	17.062 (2)	367.43 (3)	0.6 (5)	99.5 (3)	0.4 (3)	0.06 (3)
PMC-1	4.9834 (2)	17.048 (1)	366.66 (2)	1.2 (5)	99.1 (2)	0.8 (2)	0.10 (4)
PMBS-1	4.9803 (4)	17.038 (2)	365.99 (4)	1.7 (5)	98.6 (3)	1.3 (3)	0.07 (3)
PMM-1	4.9563 (2)	16.909 (1)	359.72 (2)	7.4 (5)	91.8 (14)	8.1 (14)	0.10 (2)
PMSD-1	4.9423 (2)	16.848 (1)	356.41 (2)	10.9 (5)	89.8 (9)	10.1 (9)	0.05 (3)
PMH-1	4.9355 (2)	16.832 (1)	355.08 (3)	12.4 (5)	88.8 (6)	11.1 (6)	0.09 (5)
PMU-1	4.9316 (2)	16.810 (1)	354.06 (2)	13.5 (5)	86.2 (13)	13.6 (12)	0.16 (5)
PMR-1	4.9141 (5)	16.706 (3)	349.38 (5)	19.3 (10)	84.1 (16)	15.7 (16)	0.13 (3)

Uncertainties (1σ) in last digit given in parentheses

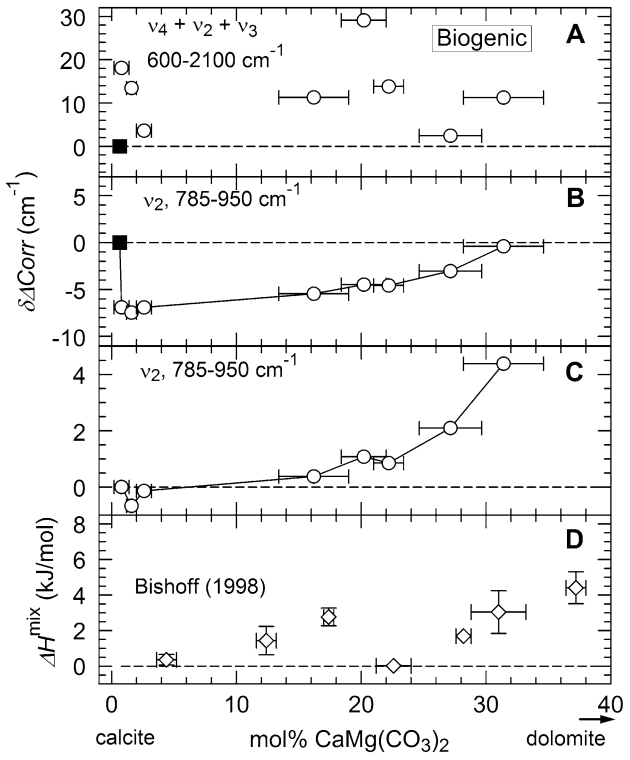

Fig. 7 **a** Autocorrelation parameter $\delta\Delta$Corr for the sum of the $\nu_4+\nu_2+\nu_3$ internal vibrations in the range of 600–2100 cm^{-1}. Values are referenced to the dashed line between inorganic calcite (solid square) and dolomite (off scale to the right). **b** $\delta\Delta$Corr for only the ν_2 internal vibrations in the range of 785–950 cm^{-1}. Values are referenced to inorganic calcite and dolomite as in (**a**). **c** Same data as in (**b**) but reference to the dashed line drawn between the most Mg-poor biogenic carbonate (PML-1, Table 4) and dolomite. **d** Enthalpy of mixing values relative to the calcite–dolomite join derived from the data of Bishoff (1998)

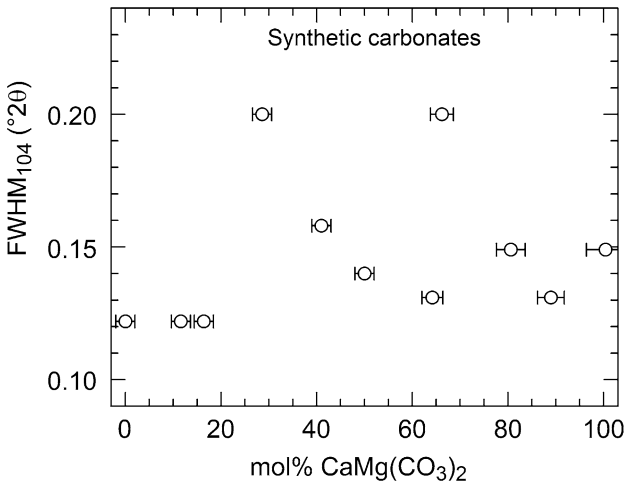

Fig. 8 Full width at half maximum (FWHM) of the 104 X-ray diffraction peak for the synthetic carbonates made in this study showing no clear correlation with composition

biogenic carbonates reported by Bishoff (1998), referenced here to the calcite–dolomite rather than the calcite–magnesite join, as shown in Fig. 7d. The main conclusion is that it is the autocorrelation of the ν_2 band that again provides the more accurate representation of the enthalpy of mixing for biogenic carbonates, perhaps owing to the relative lack of fine structure of this band in powder FTIR patterns that allows the crystal-strain broadening to be revealed.

Discussion

Comparison of the δΔCorr parameter with other measures of strain

Several other techniques have been used to study the strain effects of Mg solid solution in calcites, namely line broadening of X-ray diffraction peaks and Raman spectroscopy.

Broadening of X-ray peaks is well known to arise from both reduction in crystal size and development of non-uniform strain (Cullity 1956, pp. 98, 264). Assuming for the moment that the synthetic carbonates formed in this study are similar in size (typically ranging from < 1 to 60 µm based on optical microscopy), a plot of the full width at half maximum (FWHM) of the strongest calcite reflection (104) versus composition might potentially reveal the sort of cation substitutional strain that is sensed by the infrared spectra. Figure 8 shows the FWHM of the 104 from Table 2 versus the carbonate composition, which indicates that there is no clear correlation. To what extent the FWHM for a given sample is controlled by crystal size versus strain requires a detailed analysis of crystal-size variation across this join which is beyond the scope of this study. One can see from Fig. 8 that information on compositionally induced strain is more readily obtained from the infrared spectra than the XRD powder pattern.

Perrin et al. (2016) presented a detailed study of the Raman spectroscopy of synthetic Mg-calcites made at 2 mol% increments from 0 to 30 mol% $MgCO_3$, and at 5 mol% increments from 30 to 50 mol% $MgCO_3$. These authors reported nearly linear shifts in the position (wavenumber) of most Raman peaks over the entire calcite–dolomite range, suggesting that certain Raman modes could be used to determine the composition of a carbonate on the calcite–dolomite join. In contrast, the FWHM values varied in a parabolic and asymmetric fashion, reaching maxima near the 30–40 mol% $MgCO_3$ compositions. The FWHM of Raman vibrational bands does not show the same decrease for the low-Mg samples as observed here with the $\delta\Delta$Corr of the infrared ν_2 and $\nu_4+\nu_2+\nu_3$ bands, indicating that the

Raman spectra are also not indicating the same strain field effects as the infrared spectra.

Enthalpy of mixing for synthetic carbonates

It is possible to estimate an enthalpy of mixing curve for the entire calcite–dolomite join if the $\delta\Delta$Corr parameter for at least one sample can be calibrated against the known enthalpy of solution for that sample. Accordingly, the sample with 6.04 mol% $MgCO_3$ from Navrotsky and Capobianco (1987) was chosen to calibrate the $\delta\Delta$Corr value for the ν_2 band of sample Mg5Ca95-1-1 which has nearly the same composition (5.8 mol% $MgCO_3$, Table 2). The enthalpy of solution of the 6.04 mol% $MgCO_3$ sample was recalculated to have a ΔH^{mix} of -3.0 (± 0.70) kJ on the basis of the double salt ($Ca_{2-x}Mg_x(CO_3)_2$, $x = 0$, 1) when referenced to calcite and the (heat treated) dolomite reported by Navrotsky and Capobianco (1987). The sub-regular or 2-parameter Margules formulation for non-ideal mixing (e.g., Spear 1995, p. 203) was adopted to model the enthalpy of mixing. From this comes:

$$\Delta H^{mix} = W_{CaMg}X_{Mg}^2X_{Ca} + W_{MgCa}X_{Ca}^2X_{Mg} \quad (3)$$

where W_{ij} are the Margules (interaction) parameters for atoms i and j and X_i is the mole fraction of atom i on the octahedral (A) crystallographic site. Using the $\delta\Delta$Corr values for the ν_2 bands calibrated to ΔH^{mix} as indicated above, a non-linear regression was done for all of the $\delta\Delta$Corr ν_2 data to Eq. (3) yielding the values of W_{CaMg} and W_{MgCa} of 59 ± 5 and -32 ± 5 kJ, respectively. Reversing the process, the derived interaction parameters were used with Eq. (3) to calculate the ΔH^{mix} boundary across the whole join, which is shown in Fig. 9. Also shown for comparison in Fig. 9 are the enthalpy of mixing data for Mg-calcites of Navrotsky and Capobianco (1987, circles) and for Ca-dolomites of Chai et al. (1995, diamonds), all expressed in terms of the double salt ($Ca_{2-x}Mg_x(CO_3)_2$, $x = 0$, 1) and relative to the calcite–dolomite (synthetic or heat treated) join.

The solid curve in Fig. 9 shows that synthetic, and presumably abiotic, carbonates between pure calcite and calcite with up to ~17 mol% $MgCO_3$ (35 mol% $MgCa(CO_3)_2$) experience a minimum in the strain energy (Fig. 5d) and a corresponding minimum in the ΔH^{mix} in this compositional region. This is supported by the minimum in the solubility of synthetic carbonates in the range of 0–10 mol% $MgCO_3$ reported by Bishoff et al. (1987), which, in turn, equates to a minimum in the excess Gibbs free energy of mixing (ΔG^{ex}) (Plummer and Mackenzie 1974; Mackenzie et al. 1983). If the interaction parameters given above are used to calculate the calcite–dolomite miscibility gap, assuming there is no excess entropy of mixing (i.e., $\Delta G^{ex} = \Delta H^{mix}$), the resultant critical-point composition of 38.6 mol% $MgCO_3$ is fairly close to the 43 mol% cited by Goldsmith and Heard (1961); however, the critical temperature is unrealistically high (~1580 °C) suggesting that the assumption $\Delta G^{ex} = \Delta H^{mix}$ is not valid and that the interaction parameters, if they are accurately calibrated, should only be used to give ΔH^{mix}.

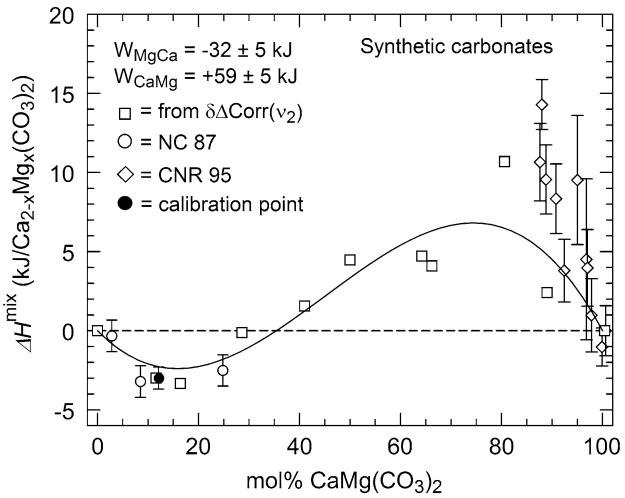

Fig. 9 Solid curve is the enthalpy of mixing (ΔH^{mix}) for the calcite–dolomite join based on a two-parameter Margules solution treatment of the autocorrelation data ($\delta\Delta$Corr, squares) derived from the ν_2 infrared band. The regressed values of W_{MgCa} and W_{CaMg} are given in the figure for the double salt. Shown for comparison are the measured values of ΔH^{mix} for magnesian calcites from Navrotsky and Capobianco (1987, NC 87, circles) and for calcian dolomites from Chai et al. (1995, CNR 95, diamonds). Solid circle was the data point of Navrotsky and Capobianco (1987) used to calibrate the $\delta\Delta$Corr data from this study

Implications for biogenic carbonate dissolution

One of the motivations of this study was to provide additional insights into the crystallographic strain energy, and therefore, solubility of biogenic carbonates for which there are conflicting results. Based on the summary of Morse et al. (2007), biogenic carbonates generally show a gradual increase in solubility with increasing $MgCO_3$ content; however, Thorstenson and Plummer (1977) observed a distinct minimum in the range of 0–5 mol% $MgCO_3$. Morse et al. (2007) noted that the data of Thorstenson and Plummer (1977) may be kinetically controlled for samples that received minimal sample preparation or thermal annealing (e.g., Walter and Morse 1984) rather than representing thermodynamic equilibrium. In this study, where the biogenic samples did not receive any special cleaning or thermal annealing, the presence of a minimum in crystallographic strain hinges on the choice of the calcite reference point. If inorganic calcite is chosen (Fig. 7b), then there is a minimum in $\delta\Delta$Corr and correspondingly a minimum in ΔH^{mix} and in the solubility comparable to synthetic carbonates (Fig. 9).

However, if the most Ca-rich biogenic carbonate is chosen (Fig. 7c), then $\delta\Delta$Corr increases steadily, with no minimum in ΔH^{mix}, and the solubility of the carbonate would gradually increase as well. As discussed above, it does not seem likely that a sudden change in $\delta\Delta$Corr would occur with the addition of only 0.4 mol% $MgCO_3$, meaning that the autocorrelation data support the gradual increase in solubility of biogenic carbonates with increasing magnesium content.

Overall, it has been found that autocorrelation analysis of carbonates in the MIR range provides an independent and reliable assessment of the crystallographic strain energy of carbonates, better than peak broadening in X-ray diffraction patterns and Raman spectra. The implications of this study on carbonates is that, in the event of growing ocean acidification (e.g., Hartin et al. 2016), biogenic carbonates in the range of 0–17 mol% $MgCO_3$ will dissolve more readily than the compositionally equivalent synthetic and (presumably) natural inorganic carbonates.

Acknowledgements Thanks are extended to R. V. Demicco for help in securing the biogenic carbonate samples used in this study and to D. Collins for help with the electron microprobe analyses and imaging. The manuscript was greatly improved by the thorough reviews of A. Benizek and M. Zhang. This work was funded by NSF Grants EAR-0947175 and EAR-1347463.

References

Althoff PL (1977) Structural refinements of dolomite and a magnesian calcite and implications for dolomite formation in the marine environment. Am Miner 62:772–783

Andersson MP, Hem CP, Schultz LN, Nielson JW, Pedersen CS, Sand KK, Okhrimenko DV, Johnsson A, Stipp SLS (2014) Infrared spectroscopy and density functional theory investigation of calcite, chalk, and coccoliths—do we observe the mineral surface? J Phys Chem A 118:10720–10729

Antao SM, Mulder WH, Hassan I, Crichton WA, Parise JB (2004) Cation disorder in dolomite, $CaMg(CO_3)_2$, and its influence on the aragonite + magnesite ↔ dolomite reaction boundary. Am Miner 89:1142–1147

Antao SM, Hassan I, Wang J, Lee PL, Toby BH (2008) State-of-the-art high-resolution powder X-ray diffraction (HRPXRD) illustrated with Rietveld structure refinement of quartz, soldalite, tremolite, and meionite. Can Miner 46:1501–1509

Bishoff WD (1998) Dissolution enthalpies of magnesian calcites. Aquat Geochem 4:321–336

Bishoff WD, Mackenzie FT, Bishop FC (1987) Stabilities of synthetic magnesian calcites in aqueous solution: comparison with biogenic materials. Geochim Cosmochim Acta 51:1413–1423

Blanch AJ, Quinton JS, Lenehan CE, Pring A (2007) Autocorrelation infrared analysis of mineralogical samples: the influence of user controllable experimental parameters. Anal Chim Acta 590:145–150

Boffa Ballaran T, Carpenter MA (2003) Line broadening and enthalpy: some empirical calibrations of solid solution behaviour from IR spectra. Phase Transit 76:137–154

Brusentsova TN, Peale RE, Maukonen D, Harlow GE, Boesenberg JS, Ebel D (2010) Far infrared spectroscopy of carbonate minerals. Am Miner 95:1515–1522

Carpenter MA (2002) Microscopic strain, macroscopic strain and the thermodynamics of phase transitions in minerals. In: Gramaccioli CM (ed) Energy modelling in minerals, EMU notes in mineral, vol 4. Eur Mineral Union, Eötvös Univ Press, Budapest, pp 311–346

Chai L, Navrotsky A, Reeder RJ (1995) Energetics of calcium-rich dolomite. Geochim Cosmochim Acta 59:939–944

Cullity BD (1956) Elements of X-ray diffraction. Addison-Wesley, Reading, p 514

Etzel K, Benisek A (2008) Thermodynamic mixing behavior of synthetic Ca-Tschermak-diopside pyroxene solid solutions: III. An analysis of IR line broadening and heat of mixing behavior. Phys Chem Miner 35:399–407

Goldsmith JR, Heard HC (1961) Subsolidus phase relations in the system $CaCO_3$–$MgCO_3$. J Geol 69:45–74

Hartin CA, Bond-Lamberty B, Patel P, Mundra A (2016) Ocean acidification over the next three centuries using a simple global climate carbon-cycle model: projections and sensitivities. Biogeosciences 13:4329–4342

Irving AJ, Wyllie PJ (1975) Subsolidus and melting relationships for calcite, magnesite and the join $CaCO_3$–$MgCO_3$ to 36 kb. Geochim Cosmochim Acta 39:35–53

Jenkins DM, Corona JC (2006) The role of water in the synthesis of glaucophane. Am Miner 91:1055–1068

Jenkins DM, Carpenter MA, Zhang M (2014) Experimental and infrared characterization of the miscibility gap along the tremolite–glaucophane join. Am Miner 99:730–741

Koch-Müller M, Mrosko M, Gottschalk M, Schade U (2012) Pressure-induced phase transitions in ilvaite studied by in situ micro-FTIR. Eur J Miner 24:831–838

Larson AC, Von Dreele RB (2004) General structure analysis system (GSAS). Los Alamos Nat Lab Report LAUR, Los Alamos, pp 86–748

Lei J, Jenkins DM, Ishida K (2015) Experimental study along the magnesio–hornblende–glaucophane join. Am Miner 100:495–509

Long X, Nasse MJ, Ma Y, Qi L (2012) From synthetic to biogenic Mg-containing calcites: a comparative study using FTIR microspectroscopy. Phys Chem Chem Phys 14:2255–2263

Mackenzie FT, Bishoff WD, Bishop FC, Loijens M, Schoonmaker J, Wollast R (1983) Magnesian calcites: low-temperature occurrence, solubility, and solid solution behavior. Rev Miner Geochem 11:97–144

Morse JW, Arvidson RS, Lüttge A (2007) Calcium carbonate formation and dissolution. Chem Rev 107:342–381

Navrotsky A, Capobianco C (1987) Enthalpies of formation of dolomite and of magnesian calcites. Am Miner 72:782–787

Perrin J, Vielzeuf D, Laporte D, Ricolleau A, Rossman GR, Floquet N (2016) Raman characterization of synthetic magnesian calcites. Am Miner 101:2525–2538

Plummer LN, Mackenzie FT (1974) Predicting mineral solubility from rate data: application to the dissolution of magnesian calcites. Am J Sci 274:61–83

Reed SJB (1996) Electron microprobe analysis and scanning electron microscopy in geology. Cambridge Univ Press, Cambridge

Reeder RJ, Nakajima Y (1982) The nature of ordering and ordering defects in dolomite. Phys Chem Miner 8:29–35

Reeder RJ, Wenk H-R (1983) Structure refinements of some thermally disordered dolomites. Am Miner 68:769–776

Robben L, Gesing TM (2013) Temperature-dependent framework-template interaction of $|Na_6(H_2O)_8|[ZnPO_4]_6$ sodalite. J Solid State Chem 207:13–20

Salje EKH, Carpenter MA, Malcherek TGW, Boffa Ballaran T (2000) Autocorrelation analysis of infrared spectra. Eur J Miner 12:503–519

Spear FS (1995) Metamorphic phase equilibria and pressure-temperature-time paths, monograph 1. Mineral Soc Amer, Washington DC

Tarantino SC, Boffa Ballaran R, Carpenter MA, Domeneghetti MC, Tazzoli V (2002) Mixing properties of the enstatite-ferrosilite solid solution: II. A microscopic perspective. Eur J Miner 14:537–547

Thorstenson DC, Plummer LN (1977) Equilibrium criteria for two-component solids reacting with fixed composition in an aqueous phase-example: the magnesian calcites. Am J Sci 277:1203–1223

Titschack J, Goetz-Neunhoeffer F, Neubauer J (2011) Magnesium quantification in calcites [(Ca,Mg)CO3] by Rietveld-based XRD analysis: revisiting a well-established method. Am Miner 96:1028–1038

Walter LM, Morse JW (1984) Magnesian calcite stabilities: a reevaluation. Geochim Cosmochim Acta 48:1059–1069

Weiner S, Dove PM (2003) An overview of biomineralization processes and the problem of the vital effect. Rev Miner Geochem 54:1–29

Wenk H-R, Zhang F (1985) Coherent transformations in calcian dolomites. Geology 13:457–460

White WB (1974) The carbonate minerals. In: Farmer VC (ed) The infrared spectra of minerals, monograph 4. Mineral Soc, London, pp 277–284

Zucchini A, Comodi P, Katerinopoulou A, Balic-Zunic T, McCammon C, Frondini F (2012) Order-disorder-reorder process in thermally treated dolomite samples: a combined powder and single-crystal X-ray diffraction study. Phys Chem Miner 39:319–328